Planet. Space Sci., Vol. 36, No. 3, pp. 291–300, 1988
Printed in Great Britain.

0032-0633/88 $3.00+0.00
Pergamon Press plc

GLOBAL RESULTS OF GRILLE SPECTROMETER EXPERIMENT ON BOARD *SPACELAB* 1

A. GIRARD, J. BESSON, D. BRARD, J. LAURENT and M. P. LEMAITRE
Office National d'Etudes et de Recherches Aérospatiales, BP 72, 92322 Châtillon Cedex, France

and

C. LIPPENS, C. MULLER, J. VERCHEVAL and M. ACKERMAN
Institut d'Aéronomie Spatiale de Belgique, 3 Avenue Circulaire, B-1180 Bruxelles, Belgique

(*Received* 14 *October* 1987)

Abstract—Measurements of atmospheric trace gases have been performed during the first *Spacelab* mission, on board the Space Shuttle, from 28 November to 8 December 1983. The principle of the observations is absorption spectroscopy, in the infrared, using the sun as a light source during sunset or sunrise periods. The instrumental set-up and the flight operations, already described in previous papers, are briefly summarized. The automatic retrieving method for the processing of the spectra is explained. Finally, all the results, in terms of vertical concentration profiles, are given for NO, NO_2, CH_4, N_2O, CO, CO_2 and H_2O. Several results have been published (Laurent *et al.*, 1985, *Nature* **315**, 126; Muller *et al.*, 1985a, *J. Optics (Paris)* **16**, 155; 1985b, *Geophys. Res. Lett.* **12**, 667; Vercheval *et al.*, 1986, *Ann. Geophys.* **4A**, 161; Laurent *et al.*, 1986, *Planet. Space Sci.* **34**, 1067). This last version may be slightly different, due to recently available and more accurate orbital parameters.

INTRODUCTION

Infrared absorption spectrometry of the atmosphere, using the sun as a light source at sunrise or sunset, has for the past 15 y proved to be a powerful method for studying vertical distributions of trace species. The largest possible amount of absorbing molecules is observed along the optical path crossing the Earth's atmosphere at various altitudes. A great deal of information has already been gathered from aircraft and balloons. An orbiting spacecraft provides access to higher altitudes and to a global coverage. Scanning of the atmosphere is also achieved at a much higher rate.

Measurements of atmospheric trace gases have been performed during the first *Spacelab* mission, on board the Space Shuttle, from 28 November to 8 December 1983 with an infrared spectrometer. This grille spectrometer has been designed by two organizations: the Office National d'Etudes et de Recherches Aérospatiales in France and the Belgian Institute for Space Aeronomy. Several descriptions of the instrument have been published (Laurent *et al.*, 1983; Lemaître *et al.*, 1984; Muller *et al.*, 1985b) and we will just give a brief summary of the set-up. Its purpose is to study, on a global scale, atmospheric composition between 15 and 150 km altitude by limb sounding.

This paper deals with a presentation, in a final form, of the vertical profiles derived from observations for NO, NO_2, N_2O, CH_4, H_2O, CO and CO_2. The comparison of these results with other measurements and with models will be presented later, separately for each species.

INSTRUMENTATION AND FLIGHT OPERATIONS

The optics consists of a two-axis steerable frontal plane mirror which tracks the sun in front of a Cassegrain telescope with aperture 30 cm and focal length 6 m. The use of a plate grille with alternate hyperbolic transparent and opaque zones at the entrance of the spectrometer provides a high luminosity (Girard and Jacquinot, 1966). A square portion of the sun (8 arc min) is imaged on the area of the grille. The spectrometer has a grating of 58 grooves per millimeter, which is illuminated by a parabolic mirror oscillating at 436 Hz, with an amplitude of ± 20 arc seconds. The position of the mirror is controlled within 5 arc seconds. The exit light flux, split into two beams, passes through interference filters to two detectors (InSb, 2.5–5.5 μm and HgCdTe, 2.5–10.5 μm). The spectral resolving power $\lambda/d\lambda$ varies between 10^4 and 2.10^4 according to the wavelength. $d\lambda$ is the instrumental line width at half peak height.

The electronics in the *Spacelab* module link the pallet instrument to the Command and Data Management System (CDMS) and the High-Rate Multiplexer (HRM). Using data originating from the

TABLE 1. LATITUDES (λ) AND LONGITUDES (ϕ) OF THE TANGENT POINTS AT 0, 50 AND 100 km FOR EACH SOLAR OCCULTATION DURING WHICH THE INSTRUMENT WAS ACTIVATED (EVENTS); THE MISSING EVENTS (1, 2, 4, 8 AND 9) CORRESPOND TO OCCULTATIONS WHERE NO SCIENTIFIC DATA COULD BE RECORDED.
The time is given for the 50 km tangent altitude, in hours, minutes and seconds; the first three digits indicate the day of the year 1983.

		0 km		50 km		100 km	
Event	Time (G.M.T.)	λ	Φ	λ	Φ	λ	Φ
3	333/23:43:18	41.43	−109.3	43.25	−110.5	45.16	−111.9
5	334/02:42:20	41.02	−153.7	42.86	−155	44.88	−156.4
6	335/09:04:02	−68.14	−132.4	−67.71	−125.4	−66.9	−118.1
7	335/12:55:47	34.87	55.74	37.41	54.32	40.15	52.63
10	336/05:10:27	30.85	172.03	33.9	170.3	37.5	168.5
11	336/08:23:46	29.78	127.83	32.86	126.3	36.19	124.5
12	336/09:53:16	29.34	105.69	32.5	104.15	35.83	102.37
13	336/12:37:13	28.33	61.48	31.61	59.91	35.1	58.08
14	337/03:47:17	22.88	−159.5	26.76	−161.2	30.89	−163.1
15	337/05:16:46	22.24	178.4	26.25	176.7	30.43	174.75
16	337/06:46:16	21.61	156.31	25.63	154.62	29.9	152.67
17	337/07:13:45	−67.16	−126.9	−67.91	−115.5	−67.77	−103.3
18	337/08:15:48	20.91	134.26	25.05	132.54	29.40	130.6
19	337/09:45:17	112.21	20.19	24.41	110.49	28.89	108.48
20	337/10:12:22	−66.96	−173.2	−67.84	−161.6	−67.8	−148.9
21	337/11:14:48	19.48	90.16	23.77	88.42	28.32	86.42
22	337/11:41:39	−66.83	163.53	−67.8	175.23	−67.81	−171.8
23	337/12:44:19	18.76	68.11	23.12	66.36	27.75	64.34

orbiter (time, attitude and orbit parameters) and from *Spacelab* (time-line, on board and ground commands, sun ephemeris), its processor manages the execution of stored measurement programs, including inflight updating. The electronics on the pallet instrument provide the functions of electromechanical control and signal detection and formatting. The pallet instrumentation weighs 122.8 kg, and the module equipment weighs 15 kg. The data rate in operation is 51.2 kilobits per second.

Among the 25 observations previously allocated to the grille spectrometer, 19 were performed which provided actually scientific data. Eighteen of them are described in Table 1, the 19th one yielding only solar spectra at altitudes where no telluric absorptions were present. Twelve were sunset occultations, seven occured at sunrise. Due to the launch data and orbit inclination, the sunset occultations were all performed at middle northern latitudes, between 23 and 43 North, while the sunrises were observed at high southern latitudes, around 68 South. Around 6000 spectra were recorded, relative to 10 different species H_2O, CO, CO_2, CH_4, N_2O, NO, NO_2, HF, HCl and O_3.

RETRIEVAL METHOD

Infrared absorption in a spectral range of a few wavenumbers is recorded for various solar elevation angles at sunset or sunrise. For each spectrum the largest height of the light path can be calculated using the geographical coordinates of the Shuttle and the position of the sun at the time of the record.

The spectral range of the spectrum has been carefully selected to contain at least one absorption line of the constituent to be detected with a minimum of overlapping by lines of other species. The spectral range can be changed with respect to a predetermined altitude to measure different species during the same sunset or sunrise.

The retrieval method is the mathematical operation which, from a set of spectra devoted to one constituent and recorded at known tangent heights, leads up to the profile of local concentration of this constituent vs altitude.

If we divide the atmosphere into concentric layers, in which temperature, pressure and concentrations are assumed to be uniform, we are able to calculate a synthetic spectrum for a given tangent height taking into account the absorption of the light in all the layers above this tangent height. For each layer one computes the line profile (Voigt profile) function of temperature and pressure for each constituent, the length of the path, taking into account the atmospheric refraction, and the strength of all the lines (function of the temperature). Introducing a first guess set of local concentrations in the layers, an absorption

spectrum through all the layers can be calculated and, by convolution with the instrumental function, degraded to the resolution of the experimental spectrum.

The retrieval program automatically compares the experimental and calculated spectra and modifies the concentration in the layers to minimize the difference between the calculated and measured spectra.

For this, we use instead of the onion peeling method, an algorithm developed by Mill (1977). The program using this algorithm has been described previously (Alamichel *et al.*, 1986). The measured spectra are first normalized with respect to the spectra with the highest tangent height; in this way, a small wavelength shift or a slope in the spectrum is corrected if necessary. Starting with a given vertical profile of concentrations, the calculated spectrum for the lowest tangent height is compared with the measured one. The concentrations at all altitudes are multiplied by a constant factor so that the next mean square difference between calculated and measured spectra is minimized, and then the process continues with the next spectrum, keeping the concentrations in the layers below this spectrum unchanged. In practice, after three iterations from the bottom to the top, a final vertical profile is obtained.

This method has many advantages:

—it takes into account all the lines of a constituent in a given spectral range, decreasing the influence of the noise in the spectrum and uncertainties in the relative strength of the lines;

—it avoids downwards noise propagation; this point is a major advantage with respect to the onion peeling technique;

—at each step of the algorithm, synthetic spectra are calculated and compared with the measured ones. The convergence of the process is fast even in the case of very non-linear variation of the absorption with respect to the concentration;

—the profiles of several constituents can be determined in the same operations.

It has been found by experiment that the final profile is practically independent from the first guess vertical profile (Alamichel *et al.*, 1986). An example of final calculated and measured spectra is given in Fig. 1.

PRESENTATION OF RESULTS

To retrieve the vertical profiles by using the automatic program, we chose a reference atmosphere, from U.S. standard 1976 for mid-latitude Spring Fall conditions. The thermospheric temperature was taken, for the low solar activity observed during the *Spacelab* flight, in order to obtain an exospheric temperature of 900 K.

This atmosphere was composed by isothermal layers of 3 km and to retrieve a profile we generally used one spectrum for each layer.

For each event, the spectra were measured from lower stratosphere to lower thermosphere (20–130 km). During these measurements, the latitude, longi-

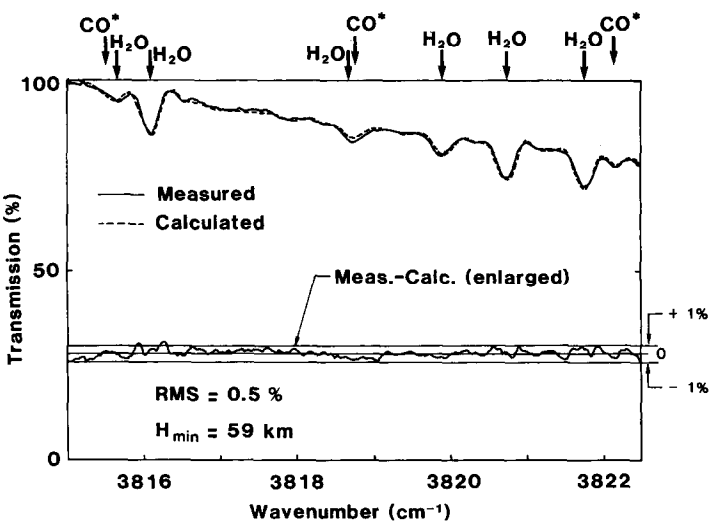

FIG. 1. EXAMPLE OF A COMPARISON BETWEEN CALCULATED AND MEASURED H_2O SPECTRUM.

tude and the altitude of the tangent point varied according to the displacement of the shuttle. For the calculations and for each spectrum, the altitude of the tangent point was taken at the time of measurement in the middle of the spectrum. The variation of the geographical position of the tangent point is reported in Table 1 for each event.

Table 2 shows the spectral intervals which were scanned and, consequently, used to retrieve the concentration profiles of every species.

A few remarks can be made from Table 2. There are three groups of profiles; H_2O, CO, NO and NO_2 profiles measured in summer at high southern latitudes, a second group with H_2O, CH_4, CO and CO_2 profiles at northern tropical latitudes, and at least H_2O, CO and N_2O profiles measured at northern mid-latitudes in winter. We can see that data concerning CO and H_2O provide a good opportunity for studying their latitudinal variations (the latitudes are indicated at 50 km altitude for H_2O and at 100 km for CO).

The concentration profiles in mol.cm^{-3} are shown in Table 3 for each species; mixing ratios are calculated using the standard atmosphere. The systematic error coming from uncertainty on parameters entering in the retrieval process, as spectral data, is not taken into account in the error bars. Figures 2–7 present mixing ratio or concentration profiles of the measured species with the envelope of the incertitude due to other effects; noise, orbit parameters uncertainty, etc. (Shaffer *et al.*, 1984).

TABLE 2. MAIN CHARACTERISTICS OF THE OBSERVATIONS. Event numbers are defined in Table 1, the altitudes indicated correspond to the ranges where vertical distributions could be inverted

Species	Event	Spectral domain (cm^{-1})	SS/SR	Z (km)
N_2O	5	2205–2211	SS	30–50
CH_4	14	3010–3020	SS	30–70
	15	2974–2982	SS	30–70
	6	1914–1918	SR	30–80
H_2O	13	3811–3825	SS	30–80
	21	3812–3825	SS	30–80
NO	6	1914.5–1918	SR	20–95
NO_2	6	1595–1598.5	SR	20–45
CO	3	2117–2123	SS	40–125
	16	2117–2123	SS	40–130
	17	2154–2162	SR	40–110
	20	2154–2162	SR	30–130
CO_2	14	2341–2348	SS	50–90
		2356–2365		90–130
	18	2341–2348	SS	50–90
		2356–2365		90–130
	21	2356–2365	SS	90–130

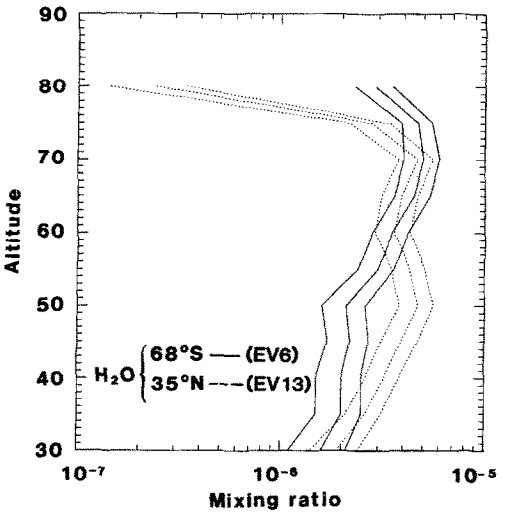

FIG. 2. MIXING RATIO PROFILES OF H_2O FOR HIGH AND MIDDLE LATITUDES.

The latitudinal variations of H_2O at high altitudes above 70 km with a higher mixing ratio in summer than in winter have to be noticed. Above this altitude it is generally assumed that there are no major chemical sources of water vapor and the dominant sink is photodissociation. The latitudinal gradient of H_2O results from upward transport by turbulent mixing and destruction by photodissociation. Otherwise, the breaking of gravity waves could be an important mechanism for turbulent mixing in the mesosphere

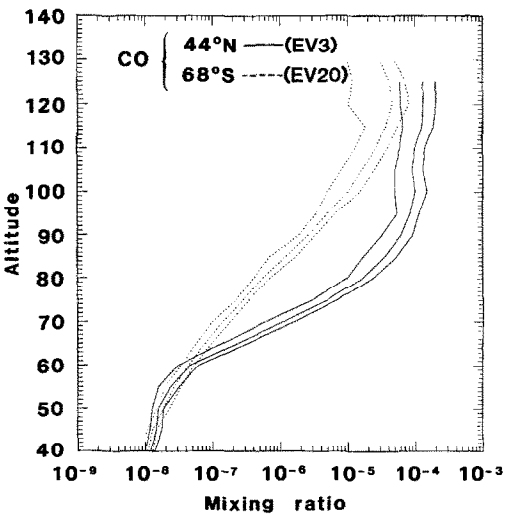

FIG. 3. MIXING RATIO PROFILES OF CO FOR HIGH AND MIDDLE LATITUDES.

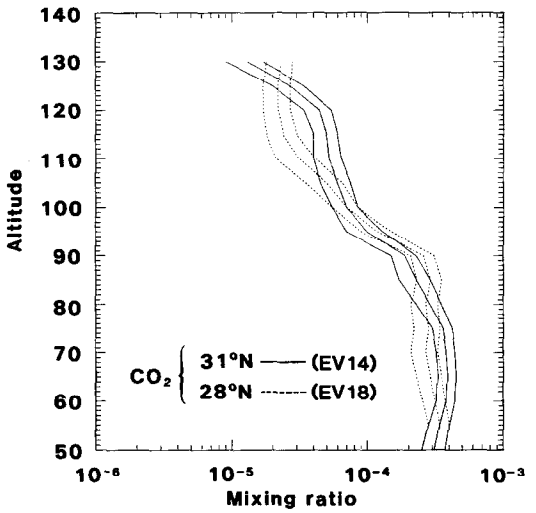

FIG. 4. MIXING RATIO PROFILES OF CO_2 NEAR 30°N.

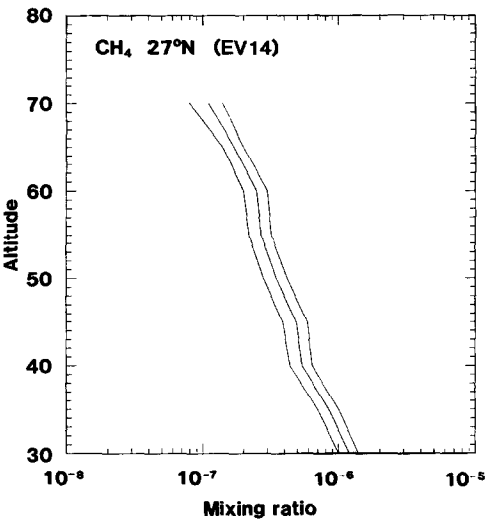

FIG. 6. MIXING RATIO PROFILE OF CH_4 NEAR 27°N.

(Holton, 1982; Solomon *et al.*, 1985) and could play a major role in the mesospheric water vapor.

The mixing ratio of CO in the middle atmosphere is dependent on both chemical and dynamical processes. In the lower thermosphere the source of CO is CO_2 photodissociation. The dominant sink is the recombination $CO+O+M \rightarrow CO_2+M$, but in this region the lifetime of CO is long and the transport at these altitudes is important. Then its abundance in the mesosphere is a balance between photochemistry and downward transport from the thermospheric source region by general circulation and eddy mixing. The CO produced in the thermospheric region is transported by downward advection in winter in the mesosphere, where the photochemical sink $CO+OH \rightarrow CO_2+H$ is low, the OH concentration being reduced in the winter mesosphere because the source of OH (H_2O photolysis) decreases rapidly.

In summer, the advection is upwards and the reaction $CO+OH \rightarrow CO_2+H$ is maximum. The latitudinal variations of CO are consistent with this competition between downward transport and photochemical destruction via OH.

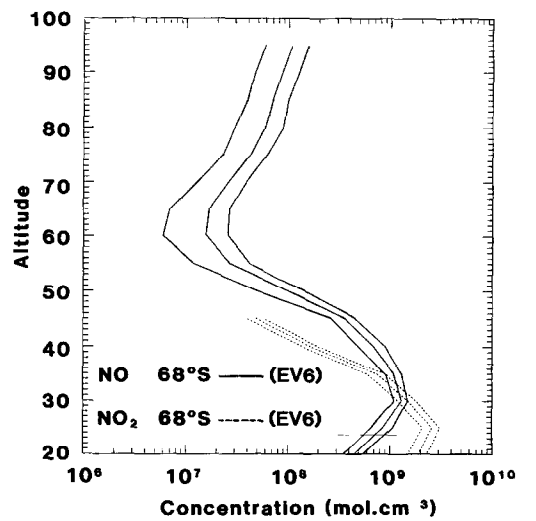

FIG. 5. SIMULTANEOUS CONCENTRATIONS PROFILES OF NO AND NO_2 AT HIGH SOUTHERN LATITUDE.

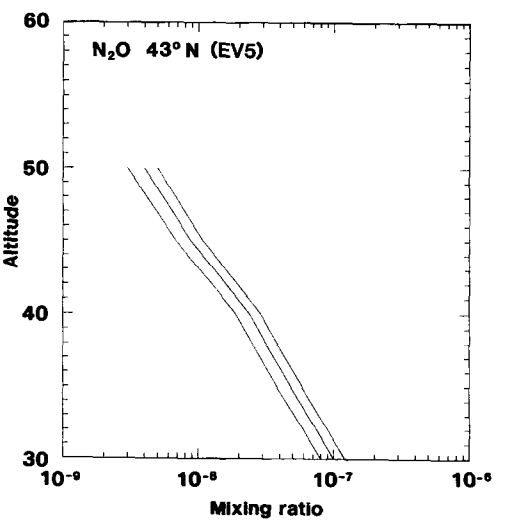

FIG. 7. MIXING RATIO PROFILE OF N_2O NEAR 43°N.

TABLE 3A. NUMERICAL DATA FOR THE VERTICAL PROFILES OF NO, NO_2 AND N_2O.
Event numbers are defined in Table 1

Altitude (km)	Concentration (mol. cm^{-3})	Mixing ratio
	NO (EV 6)	
20	$(0.45\pm0.10)\times10^{9}$	0.24 ± 0.05 ppb
25	$(0.87\pm0.20)\times10^{9}$	1.0 ± 0.02 ppb
30	$(0.13\pm0.02)\times10^{10}$	3.4 ± 0.05 ppb
35	$(0.11\pm0.02)\times10^{10}$	6.3 ± 1.1 ppb
40	$(0.70\pm0.20)\times10^{9}$	8.4 ± 2.5 ppb
45	$(0.37\pm0.10)\times10^{9}$	9.0 ± 3.0 ppb
50	$(0.10\pm0.05)\times10^{9}$	4.7 ± 2.5 ppb
55	$(0.27\times0.15)\times10^{8}$	2.3 ± 1.3 ppb
60	$(0.16\pm0.10)\times10^{8}$	2.5 ± 1.5 ppb
65	$(0.17\pm0.10)\times10^{8}$	4.9 ± 3.0 ppb
70	$(0.26\pm0.13)\times10^{8}$	14.0 ± 7.0 ppb
75	$(0.43\pm0.20)\times10^{8}$	48.0 ± 20.0 ppb
80	$(0.60\pm0.30)\times10^{8}$	0.14 ± 0.07 ppm
85	$(0.70\pm0.30)\times10^{8}$	0.41 ± 0.20 ppm
90	$(0.87\pm0.40)\times10^{8}$	1.2 ± 0.6 ppm
95	$(0.11\pm0.05)\times10^{9}$	3.7 ± 2.0 ppm
	NO_2(EV 6)	
20	$(0.19\pm0.04)\times10^{10}$	1.0 ± 0.2 ppb
25	$(0.26\pm0.05)\times10^{10}$	3.1 ± 0.6 ppb
30	$(0.15\pm0.03)\times10^{10}$	3.9 ± 0.8 ppb
35	$(0.75\pm0.15)\times10^{9}$	4.3 ± 0.8 ppb
40	$(0.17\pm0.03)\pm10^{9}$	2.1 ± 0.4 ppb
45	$(0.50\pm0.10)\times10^{8}$	1.2 ± 0.2 ppb
	N_2O (EV 5)	
30	$(0.38\pm0.08)\times10^{11}$	100.0 ± 20.0 ppb
35	$(0.85\pm0.17)\times10^{10}$	48.0 ± 10.0 ppb
40	$(0.20\pm0.04)\times10^{10}$	24.0 ± 5.0 ppb
45	$(0.36\pm0.08)\times10^{9}$	8.8 ± 2.0 ppb
50	$(0.85\pm0.20)\times10^{8}$	4.0 ± 1.0 ppb

TABLE 3B. NUMERICAL DATA FOR THE VERTICAL PROFILES OF H_2O.
Event numbers are defined in Table 1

Altitude (km)	Concentration (mol. cm^{-3})	Mixing ratio
	H_2O)EV 6)	
30	$(0.6\pm0.20)\times10^{12}$	1.6 ± 0.5 ppm
35	$(0.33\pm0.08)\times10^{12}$	2.0 ± 0.5 ppm
40	$(0.17\pm0.04)\times10^{12}$	2.0 ± 0.5 ppm
45	$(0.90\perp0.20)\times10^{11}$	$2.2\perp0.5$ ppm
50	$(0.45\pm0.10)\times10^{11}$	2.1 ± 0.5 ppm
55	$(0.30\pm0.06)\times10^{11}$	3.0 ± 0.6 ppm
60	$(0.22\pm0.04)\times10^{11}$	3.5 ± 0.7 ppm
65	$(0.155\pm0.03)\times10^{11}$	4.5 ± 0.9 ppm
70	$(0.90\pm0.20)\times10^{10}$	5.0 ± 1.0 ppm
75	$(0.42\pm0.07)\times10^{10}$	4.7 ± 0.8 ppm
80	$(0.12\pm0.03)\times10^{10}$	2.9 ± 0.6 ppm
	H_2O (EV 13)	
30	$(0.72\pm0.20)\times10^{12}$	1.9 ± 0.5 ppm
35	$(0.45\pm0.10)\times10^{12}$	2.6 ± 0.5 ppm
40	$(0.27\pm0.05)\times10^{12}$	3.2 ± 0.6 ppm
45	$(0.16\pm0.03)\times10^{12}$	3.9 ± 0.8 ppm
50	$(0.10\pm0.02)\times10^{12}$	4.7 ± 0.9 ppm
55	$(0.50\pm0.10)\times10^{11}$	4.3 ± 0.8 ppm
60	$(0.23\pm0.04)\times10^{11}$	3.6 ± 0.7 ppm
65	$(0.135\pm0.03)\times10^{11}$	3.9 ± 0.8 ppm
70	$(0.85\pm0.17)\times10^{10}$	4.7 ± 0.9 ppm
75	$(0.25\pm0.05)\times10^{10}$	2.8 ± 0.6 ppm
80	$(0.10\pm0.04)\times10^{9}$	0.24 ± 0.1 ppm
	H_2O (EV 21)	
30	$(0.65\pm0.20)\times10^{12}$	1.7 ± 0.5 ppm
35	$(0.45\pm0.10)\times10^{12}$	2.6 ± 0.5 ppm
40	$(0.32\pm0.06)\times10^{12}$	3.9 ± 0.8 ppm
45	$(0.19\pm0.04)\times10^{12}$	4.6 ± 1.0 ppm
50	$(0.10\pm0.02)\times10^{12}$	4.7 ± 1.0 ppm
55	$(0.52\pm0.10)\times10^{11}$	4.4 ± 0.9 ppm
60	$(0.28\pm0.06)\times10^{11}$	4.4 ± 0.9 ppm
65	$(0.16\pm0.03)\times10^{11}$	4.6 ± 0.65 ppm
70	$(0.65\pm0.13)\times10^{10}$	3.6 ± 0.7 ppm
75	$(0.20\pm0.05)\times10^{10}$	2.3 ± 0.6 ppm
80	$(0.20\pm0.08)\times10^{9}$	0.49 ± 0.2 ppm

TABLE 3C. NUMERICAL VALUES FOR THE VERTICAL PROFILES OF CH_4.
Event numbers are defined in Table 1

Altitude (km)	Concentration (mol. cm^{-3})	Mixing ratio
	CH_4 (EV 14)	
30	$(0.45 \pm 0.08) \times 10^{12}$	1.2 ± 0.2 ppm
35	$(0.15 \pm 0.03) \times 10^{12}$	0.85 ± 0.15 ppm
40	$(0.45 \pm 0.10) \times 10^{11}$	0.54 ± 0.1 ppm
45	$(0.20 \pm 0.04) \times 10^{11}$	0.49 ± 0.1 ppm
50	$(0.75 \pm 0.15) \times 10^{10}$	0.35 ± 0.07 ppm
55	$(0.32 \pm 0.06) \times 10^{10}$	0.27 ± 0.05 ppm
60	$(0.16 \pm 0.03) \times 10^{10}$	0.25 ± 0.05 ppm
65	$(0.60 \pm 0.12) \times 10^{9}$	0.17 ± 0.03 ppm
70	$(0.20 \pm 0.05) \times 10^{9}$	0.11 ± 0.03 ppm
	CH_4 (EV 15)	
30	$(0.5 \pm 0.08) \times 10^{12}$	1.3 ± 0.2 ppm
35	$(0.18 \pm 0.03) \times 10^{12}$	1.0 ± 0.2 ppm
40	$(0.70 \pm 0.15) \times 10^{11}$	0.84 ± 0.2 ppm
45	$(0.27 \pm 0.04) \times 10^{11}$	0.66 ± 0.1 ppm
50	$(0.11 \pm 0.02) \times 10^{11}$	0.51 ± 0.1 ppm
55	$(0.42 \pm 0.08) \times 10^{10}$	0.36 ± 0.07 ppm
60	$(0.17 \pm 0.03) \times 10^{10}$	0.27 ± 0.05 ppm
65	$(0.75 \pm 0.15) \times 10^{10}$	0.22 ± 0.05 ppm
70	$(0.25 \pm 0.05) \times 10^{9}$	0.14 ± 0.03 ppm

TABLE 3D. NUMERICAL VALUES FOR THE VERTICAL PROFILES OF CO.
Event numbers are defined in Table 1

Altitude (km)	Concentration (mol. cm^{-3})	Mixing ratio
	CO (EV 3)	
40	$(0.10 \pm 0.02) \times 10^{10}$	12.00 ± 2.00 ppb
45	$(0.60 \pm 0.12) \times 10^{9}$	15.00 ± 3.00 ppb
50	$(0.35 \pm 0.07) \times 10^{9}$	16.0 ± 3.0 ppb
55	$(0.28 \pm 0.10) \times 10^{9}$	24.0 ± 8.0 ppb
60	$(0.30 \pm 0.10) \times 10^{9}$	47.0 ± 16.0 ppb
65	$(0.80 \pm 0.30) \times 10^{9}$	0.23 ± 0.09 ppm
70	$(0.20 \pm 0.10) \times 10^{10}$	1.1 ± 0.5 ppm
75	$(0.45 \pm 0.20) \times 10^{10}$	5.0 ± 2.0 ppm
80	$(0.70 \pm 0.30) \times 10^{10}$	17.0 ± 7.0 ppm
85	$(0.60 \pm 0.30) \times 10^{10}$	35.0 ± 18.0 ppm
90	$(0.45 \pm 0.20) \times 10^{10}$	62.0 ± 30.0 ppm
95	$(0.25 \pm 0.10) \times 10^{10}$	84.0 ± 30.0 ppm
100	$(0.13 \pm 0.07) \times 10^{10}$	100.0 ± 50.0 ppm
105	$(0.50 \pm 0.20) \times 10^{9}$	90.0 ± 40.0 ppm
110	$(0.25 \pm 0.10) \times 10^{9}$	100.0 ± 40.0 ppm
115	$(0.14 \pm 0.07) \times 10^{9}$	125.0 ± 60.0 ppm
120	$(0.70 \pm 0.30) \times 10^{8}$	130.0 ± 70.0 ppm
125	$(0.40 \pm 0.20) \times 10^{8}$	130.0 ± 70.0 ppm
	CO (EV 16)	
40	$(0.90 \pm 0.02) \times 10^{9}$	11.0 ± 2.00 ppb
45	$(0.45 \pm 0.10) \times 10^{9}$	11.0 ± 2.00 ppb
50	$(0.30 \pm 0.07) \times 10^{9}$	14.0 ± 3.0 ppb
55	$(0.17 \pm 0.05) \times 10^{9}$	15.0 ± 6.0 ppb
60	$(0.17 \pm 0.05) \times 10^{9}$	27.0 ± 8.0 ppb
65	$(0.35 \pm 0.10) \times 10^{9}$	0.10 ± 0.03 ppm
70	$(0.65 \pm 0.20) \times 10^{9}$	0.36 ± 0.12 ppm
75	$(0.75 \pm 0.30) \times 10^{9}$	0.84 ± 0.3 ppm
80	$(0.70 \pm 0.30) \times 10^{9}$	1.7 ± 0.7 ppm
85	$(0.60 \pm 0.30) \times 10^{9}$	3.5 ± 1.8 ppm
90	$(0.46 \pm 0.20) \times 10^{9}$	6.4 ± 3.0 ppm
95	$(0.35 \pm 0.07) \times 10^{9}$	12.0 ± 2.5 ppm
100	$(0.27 \pm 0.10) \times 10^{9}$	21.0 ± 8.0 ppm
105	$(0.20 \pm 0.10) \times 10^{9}$	36.0 ± 18.0 ppm
110	$(0.14 \pm 0.07) \times 10^{9}$	56.0 ± 30.0 ppm
115	$(0.70 \pm 0.30) \times 10^{8}$	62.0 ± 30.0 ppm
120	$(0.30 \pm 0.15) \times 10^{8}$	54.0 ± 30.0 ppm
125	$(0.10 \pm 0.05) \times 10^{8}$	32.0 ± 16.0 ppm
130	$(0.30 \pm 0.20) \times 10^{7}$	15.0 ± 10.0 ppm

TABLE 3E. NUMERICAL VALUES FOR THE VERTICAL PROFILES OF CO.
Event numbers are defined in Table 1

Altitude (km)	Concentration (mol. cm^{-3})	Mixing ratio
	CO (EV 17)	
40	$(0.11 \pm 0.02) \times 10^{10}$	13.00 ± 2.00 ppb
45	$(0.45 \pm 0.10) \times 10^{9}$	11.0 ± 2.00 ppb
50	$(0.30 \pm 0.07) \times 10^{9}$	14.0 ± 8.0 ppb
55	$(0.25 \pm 0.06) \times 10^{9}$	21.0 ± 5.0 ppb
60	$(0.22 \pm 0.06) \times 10^{9}$	35.0 ± 10.0 ppb
65	$(0.20 \pm 0.05) \times 10^{9}$	58.0 ± 15.0 ppb
70	$(0.20 \pm 0.05) \times 10^{9}$	0.11 ± 0.05 ppm
75	$(0.20 \pm 0.05) \times 10^{9}$	0.22 ± 0.05 ppm
80	$(0.20 \pm 0.05) \times 10^{9}$	0.49 ± 0.12 ppm
85	$(0.20 \pm 0.05) \times 10^{9}$	1.1 ± 0.5 ppm
90	$(0.19 \pm 0.05) \times 10^{9}$	2.6 ± 0.7 ppm
95	$(0.17 \pm 0.05) \times 10^{9}$	5.7 ± 1.6 ppm
100	$(0.15 \pm 0.05) \times 10^{9}$	12.0 ± 4.0 ppm
105	$(0.14 \pm 0.05) \times 10^{9}$	26.0 ± 10.0 ppm
110	$(0.12 \pm 0.05) \times 10^{9}$	48.0 ± 20.0 ppm
	CO (EV 20)	
40	$(0.25 \pm 0.05) \times 10^{10}$	11.00 ± 2.00 ppb
45	$(0.15 \pm 0.03) \times 10^{10}$	13.0 ± 2.00 ppb
50	$(0.95 \pm 0.20) \times 10^{9}$	19.0 ± 4.0 ppb
55	$(0.55 \pm 0.10) \times 10^{9}$	27.0 ± 7.0 ppb
60	$(0.28 \pm 0.07) \times 10^{9}$	44.0 ± 10.0 ppb
65	$(0.27 \pm 0.07) \times 10^{9}$	78.0 ± 20.0 ppb
70	$(0.26 \pm 0.07) \times 10^{9}$	0.14 ± 0.04 ppm
75	$(0.25 \pm 0.06) \times 10^{9}$	0.28 ± 0.06 ppm
80	$(0.23 \pm 0.06) \times 10^{9}$	0.56 ± 0.15 ppm
85	$(0.21 + 0.05) \times 10^{9}$	1.2 ± 0.5 ppm
90	$(0.19 \pm 0.05) \times 10^{9}$	2.6 ± 0.7 ppm
95	$(0.15 \pm 0.05) \times 10^{9}$	5.0 ± 1.6 ppm
100	$(0.12 \pm 0.05) \times 10^{9}$	10.0 ± 5.0 ppm
105	$(0.90 \pm 0.50) \times 10^{8}$	16.0 ± 8.0 ppm
110	$(0.65 \pm 0.30) \times 10^{8}$	26.0 ± 13.0 ppm
115	$(0.40 \pm 0.20) \times 10^{8}$	36.0 ± 18.0 ppm
120	$(0.25 \pm 0.20) \times 10^{8}$	45.0 ± 35.0 ppm
125	$(0.13 \pm 0.10) \times 10^{8}$	42.0 ± 30.0 ppm
130	$(0.60 \pm 0.40) \times 10^{7}$	30.0 ± 20.0 ppm

TABLE 3F. NUMERICAL VALUES FOR THE VERTICAL PROFILES OF CO_2.
Event numbers are defined in Table 1

Altitude (km)	Concentration (mol. cm^{-3})	Mixing ratio
	CO_2 (EV 14)	
50	$(0.65 \pm 0.10) \times 10^{13}$	310.0 ± 60.0 ppm
55	$(0.40 \pm 0.06) \times 10^{13}$	340.0 ± 60.0 ppm
60	$(0.24 \pm 0.04) \times 10^{13}$	380.0 ± 60.0 ppm
65	$(0.14 \pm 0.02) \times 10^{13}$	390.0 ± 60.0 ppm
70	$(0.70 \pm 0.14) \times 10^{12}$	380.0 ± 60.0 ppm
75	$(0.32 \pm 0.05) \times 10^{12}$	360.0 ± 60.0 ppm
80	$(0.12 \pm 0.025) \times 10^{12}$	290.0 ± 60.0 ppm
85	$(0.40 \pm 0.08) \times 10^{11}$	230.0 ± 60.0 ppm
90	$(0.14 \pm 0.03) \times 10^{11}$	190.0 ± 40.0 ppm
95	$(0.30 \pm 0.10) \times 10^{10}$	100.0 ± 30.0 ppm
100	$(0.90 \pm 0.20) \times 10^{9}$	70.0 ± 15.0 ppm
105	$(0.33 \pm 0.08) \times 10^{9}$	60.0 ± 15.0 ppm
110	$(0.13 \pm 0.03) \times 10^{9}$	52.0 ± 12.0 ppm
115	$(0.56 \pm 0.11) \times 10^{8}$	50.0 ± 10.0 ppm
120	$(0.24 \pm 0.06) \times 10^{8}$	44.0 ± 10.0 ppm
125	$(0.85 \pm 0.20) \times 10^{7}$	27.0 ± 7.0 ppm
130	$(0.24 \pm 0.06) \times 10^{7}$	13.0 ± 4.0 ppm
	CO_2 (EV 18)	
50	$(0.65 \pm 0.10) \times 10^{13}$	310.0 ± 60.0 ppm
55	$(0.35 \pm 0.06) \times 10^{13}$	340.0 ± 60.0 ppm
60	$(0.20 \pm 0.04) \times 10^{13}$	315.0 ± 60.0 ppm
65	$(0.10 \pm 0.02) \times 10^{13}$	290.0 ± 60.0 ppm
70	$(0.50 \pm 0.10) \times 10^{12}$	270.0 ± 60.0 ppm
75	$(0.25 \pm 0.05) \times 10^{12}$	280.0 ± 60.0 ppm
80	$(0.11 \pm 0.025) \times 10^{12}$	270.0 ± 60.0 ppm
85	$(0.50 \pm 0.10) \times 10^{11}$	290.0 ± 60.0 ppm
90	$(0.19 \pm 0.04) \times 10^{11}$	260.0 ± 50.0 ppm
95	$(0.35 \pm 0.10) \times 10^{10}$	120.0 ± 30.0 ppm
100	$(0.90 \pm 0.20) \times 10^{9}$	70.0 ± 15.0 ppm
105	$(0.28 \pm 0.08) \times 10^{9}$	50.0 ± 15.0 ppm
110	$(0.78 \pm 0.25) \times 10^{8}$	31.0 ± 10.0 ppm
115	$(0.27 \pm 0.07) \times 10^{8}$	24.0 ± 6.0 ppm
120	$(0.12 \pm 0.03) \times 10^{8}$	22.0 ± 5.0 ppm
125	$(0.70 \pm 0.20) \times 10^{7}$	22.0 ± 5.0 ppm
130	$(0.45 \pm 0.15) \times 10^{7}$	23.0 ± 5.0 ppm

TABLE 3G. NUMERICAL VALUES FOR THE VERTICAL PROFILES OF CO_2.
Event numbers are defined in Table 1

	CO_2 (EV 21)	
90	$(0.20 \pm 0.04) \times 10^{11}$	280.0 ± 50.0 ppm
95	$(0.40 \pm 0.10) \times 10^{10}$	135.0 ± 30.0 ppm
100	$(0.95 \pm 0.20) \times 10^{9}$	75.0 ± 15.0 ppm
105	$(0.26 \pm 0.08) \times 10^{9}$	47.0 ± 15.0 ppm
110	$(0.90 \pm 0.20) \times 10^{8}$	36.0 ± 10.0 ppm
115	$(0.40 \pm 0.10) \times 10^{8}$	35.0 ± 8.0 ppm
120	$(0.19 \pm 0.05) \times 10^{8}$	35.0 ± 10.0 ppm
125	$(0.11 \pm 0.03) \times 10^{8}$	35.0 ± 10.0 ppm
130	$(0.70 \pm 0.20) \times 10^{7}$	36.0 ± 10.0 ppm

The CO_2 profiles show a quasi-constant profile until 90 km at 340 ppm and then a rapid decrease due to its photodissociation. This reduction reaches about a factor 10 between 90 and 125 km and relates to the CO mixing ratios measured on the lower thermosphere.

As for CO, NO is produced in the thermosphere and destroyed in the summer mesosphere. In the thermosphere, the rate of production of NO is strongly dependent on ionization, solar activity and branching ratio between the production of $N(^4S)$ and $N(^2D)$. In the lower mesosphere and upper stratosphere, NO is destroyed by $NO + N(^4S)$. The high maximum of NO observed at 90 km must be a consequence of the competition between the highly variable production of NO in the thermosphere and, in this case, the upward advection in summer (68°S).

At last, the NO_2, CH_4 and N_2O profiles are consistent with previous balloon, rocket and satellite observations and with what is known of their photochemistry (Laurent *et al.*, 1985; Muller *et al.*, 1985b).

CONCLUSION

The set of data presented in this paper is derived from observations collected during the 10 day mission of the first *Spacelab* payload. Observations have been performed for the first time through the whole middle atmosphere over a wide range of latitude and seasons, on a set of trace constituents of basic importance to the knowledge of photochemistry and transport processes occuring in the middle atmosphere. The results cover the whole of the spectral observations related to NO, NO_2, CH_4, N_2O, CO, CO_2 and H_2O. Other data related to O_3, HCl and HF have still to be processed.

Though severely limited in number, these results are very significant due to the high level of confidence commonly associated with infrared spectrometry used in the absorption mode according to the solar occultation technique. So, these results illustrate the specific advantages of short repetitive satellite missions:

- —highly sensitive instrumentation specially adapted to short missions; for example, a relatively simple cryogenic device was used for cooling the infrared detectors;
- —possibility of preflight and postflight ground-based calibration;
- —flexibility in the scientific program coming from the interaction between experimenters NASA–ESA mission scientists and crew during the mission. This interaction was surprisingly efficient during the first *Spacelab* mission.

A second mission, using the same equipment, was planned for September 1986, in the framework of the ATLAS 1 mission. The autonomy of the cryogenic device, which is the main constraint limiting the number of observations, has been increased by a factor of five, owing to the technical help of NASA.

Now, as a consequence of the *Challenger* disaster, the next flight is planned for mid-1991.

REFERENCES

Alamichel, C., Laurent, J., Brard, D. and Mendez, F. (1986) An automatic program for retrieving atmospheric mixing ratio profiles from occultation spectra. *Ann. Geophys.* **4**, 201.

Girard, A. and Jacquinot, P. (1966) Principles of instrumental methods in spectroscopy, in *Advanced Optical Techniques* (Edited by Van Heel, A. C. S.). North Holland, Rotterdam.

Holton, J. R. (1982) The role of gravity wave induced drag and diffusion in the momentum budget of the mesosphere. *J. atmos. Sci.* **39**, 791.

Laurent, J., Brard, D., Girard, A., Camy-Peyret, C., Lippens, C., Muller, C., Vercheval, J. and Ackerman, M. (1986) Middle atmospheric water vapor observed by the *Spacelab* One grille spectrometer. *Planet. Space Sci.* **34**, 1067.

Laurent, J., Lemaitre, M. P., Besson, J., Girard, A., Lippens, C., Muller, C., Vercheval, J. and Ackerman, M. (1985) Middle atmospheric NO and NO_2 observed by the *Spacelab* grille spectrometer. *Nature* **315**, 126.

Laurent, J., Lemaitre, M. P., Lippens, C. and Muller, C. (1983) Expérience de spectrométrie infrarouge pour la première mission *Spacelab*. *l'Aéronautique et l'Astronautique* **98**, 1.

Lemaître, M. P., Laurent, J., Besson, J., Girard, A., Muller, C., Lippens, C., Vercheval, J. and Ackerman, M. (1984) A sample performance of the grille spectrometer on board *Spacelab*. *Science* **225**, 171.

Mill, J. D. (1977) An efficient method for inverting limb radiance profiles with application to the fluorocarbons. Ph.D. Thesis, University of Michigan, Ann Arbor.

Muller, C., Lippens, C., Vercheval, J., Ackerman, M., Laurent, J., Lemaitre, M. P., Besson, J. and Girard, A. (1985a) Expérience "spectromètre à grille" à bord de la première charge utile de *Spacelab*. *J. Optics (Paris)* **16**, 155.

Muller, C. Vercheval, J. Ackerman, M., Lippens, C.,

Laurent, J., Lemaitre, M. P., Besson, J. and Girard, A. (1985b) Observations of middle atmospheric CH_4 and N_2O vertical distributions by the *Spacelab* 1 grille spectrometer. *Geophys. Res. Lett.* **12**, 667.

Shaffer, W. A., Shaw, J. H. and Farmer, C. B. (1984) Effects of systematic errors on the mixing ratios of gases obtained from occultation spectra. *Appl. Optics* **23**, 2818.

Solomon, S., Garcia, R. R., Olivero, J. J., Bevilacqua, R. M., Schwartz, P. R., Clancy, R. T. and Muhleman, D. O. (1985) Photochemistry and transport of carbon monoxide in the middle atmosphere. *J. atmos. Sci.* **42**, 1072.

Vercheval, J., Lippens, C., Muller, C., Ackerman, M., Lemaitre, M. P., Besson, J., Girard, A. and Laurent, J. (1986) CO_2 and CO vertical distribution in the middle atmosphere and lower thermosphere deduced from infrared spectra. *Ann. Geophys.* **4A**, 161.